Raman calibration of the HT-7 yttrium aluminum garnet Thomson scattering for electron density measurements

Qing Zang,[a] Junyu Zhao, Xiang Gao, Lingwei Shi, Tao Zhang, Xiaoqi Xi, Li Yang, Qingsheng Hu, and S. Sajjad
Institute of Plasma Physics, Chinese Academy of Sciences, P.O. Box 1126, Hefei, Anhui 230031, People's Republic of China

(Received 31 July 2007; accepted 22 October 2007; published online 30 November 2007)

A multipulse neodym doped yttrium aluminum garnet laser Thomson scattering system calibrated by the anti-Stokes rotational Raman scattering from nitrogen gas had been developed in the HT-7 superconducting Tokmak. By virtue of this system, measured electron density results of the plasma were obtained. The results showed good repeatability and its total uncertainty was estimated to be ±18%. © *2007 American Institute of Physics.* [DOI: 10.1063/1.2813895]

I. INTRODUCTION

Thomson scattering (TS) is a powerful diagnostic technique for determining the fundamental plasma parameters such as the electron temperature T_e and the electron density n_e. Recently, a developed multipulse Nd:YAG (yttrium aluminum garnet) TS system has been developed instead of Nd:glass laser TS system.[1] In our previous work, this system was applied on HT-7 Tokamak for T_e measurements.[2] However, n_e of the plasma could not be obtained due to the lack of absolute calibration.

Raman scattering offers many advantages for calibrating HT-7 Tokmak system, owing to that Raman scattering light meets the wavelength demand of the filters in TS equipment.[3] Also, Raman scattering calibration is not affected by the scattering of microparticle dust. Moreover, the intensity of Raman scattering was similar to that of Thomson scattering.[4] Thus, the accuracy of the calibration increased as the detector could be directly adapted without changing any characteristic of the system. The rotational Raman scattering is an ideal choice for the calibration of the Tokmaks.

In the literature, SF_6,[5] hydrogen,[4,6] deuterium,[6] nitrogen,[7] and air[8] rotational Raman scatterings have been proposed and employed. However, there is little description of Raman scattering experiment from nitrogen gas on Tokmaks with Nd:YAG laser TS system.

In this article, the anti-Stokes Raman-scattered light from nitrogen gas of 1064 nm incident laser has been used to calibrate particular channels of the TS system on HT-7 Tokmak. The calibration procedure and error estimation were described in detail. At the same time, the relationship between the Raman and Thomson scattering signals has been discussed. Lastly, an interesting example of electron density of the center plasma of HT-7 measured by the calibrated Thomson scattering system was shown.

[a]Author to whom correspondence should be addressed. Tel.: 86-551-5591394. Electronic mail: zangq@ipp.ac.cn

II. HT-7 THOMSON SCATTERING DEVICE

The TS experimental setup on HT-7 Tokmak has been shown in Fig. 1. This system employs Nd:YAG laser as the source. The laser works at the fundamental wavelength of $\lambda = 1064$ nm. The pulse energy is about 1.8 J, the pulse duration is 6–10 ns, and the repetition rate is 10 Hz. The laser light reaches the input optics in the lower pit underneath the HT-7, and then passes through the plasma vertically. The Thomson scattering light is collected by a collection lens which images the laser beam on a 1.5×4 mm^2 fiber optic bundle comprised of about 200 low loss quartz fibers with a diameter of 150 μm. Afterwards, the 2.3 mm diameter output light from the other side of the fiber passes through every filter sequentially and images onto each one of the five sensitive detectors in the polychromator.

The basic design of the polychromator is presented in Fig. 2. Basically, one polychromator box is made up of five interference filters. These filters are directly coupled to a silicon avalanche, allowing the scattered light to transmit at a certain wavelength. Each polychromator channel also equips

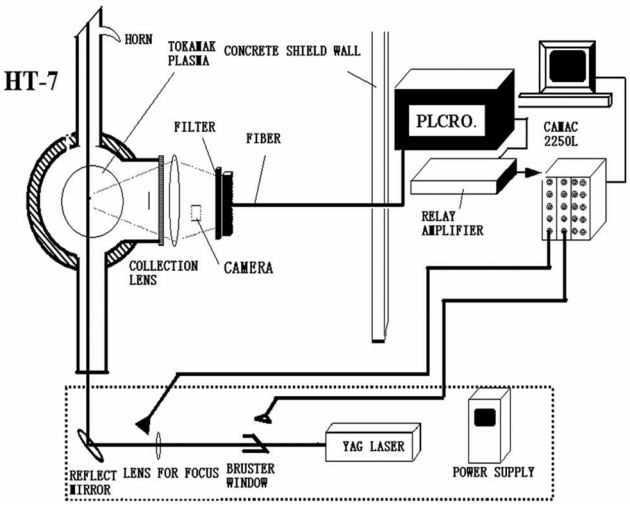

FIG. 1. Thomson scattering experimental setup on HT-7 Tokmak.

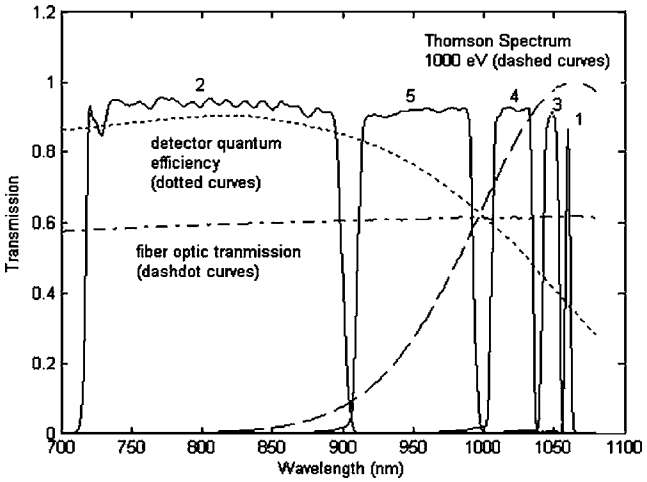

FIG. 2. Measured transmission curves (solid) for the polychromator. The number of the curve indicates the sequence of the corresponding filter in the polychromator. Also shown are the measured fiber optic transmission (dash dot), the measured detector quantum efficiency (dotted), and 1000 eV Thomson spectrum.

an amplifier and a filter circuit in order to detect the small number of photons. Consequently, we can get the higher frequency signal while rejecting the lower frequency background light. The output signal from amplified circuit containing the scattering light information is digitized with LeCrroy2250L charge sensitive fast buffered 12-channel analog to digital converter.

The experimental setup is identical in both the Thomson and Raman scattering measurements, except that the HT-7 vacuum vessel is filled with nitrogen for the Raman calibration.

III. BASIC FORMULA FOR RAMAN CALIBRATION AND RAMAN EXPERIMENTAL PROCEDURE

The intensity of Thomson scattering signal can be written as[4]

$$S^T = AEn_e \frac{d\sigma^T}{d\Omega} \int S(\lambda, T_e) f_1(\lambda) d\lambda, \tag{1}$$

$S(\lambda)$ is the power function of Thomson scattering in the noncooperative regime, when the relativistic effects are taken into account, it is given by[9,10]

$$S(\Delta\lambda, T_e) = \frac{A_0}{\sin\left(\frac{\theta}{2}\right)\sqrt{T_e}\lambda_0}\left[1 - 3.5\frac{\Delta\lambda}{\lambda_0} + \frac{B_0\Delta\lambda}{\sin^2\left(\frac{\theta}{2}\right)T_e}\left(\frac{\Delta\lambda}{\lambda_0}\right)^2\right] \times \exp\left[-\left(\frac{\Delta\lambda}{\lambda_0}\right)^2 \frac{B_0}{\sin^2\left(\frac{\theta}{2}\right)T_e}\left(1 - \frac{\Delta\lambda}{\lambda_0}\right)\right], \tag{2}$$

where

$$\Delta\lambda = \lambda_0 - \lambda,$$

$$A_0 = \frac{c}{2\pi^{1/2}(2k/m_e)^{1/2}},$$

$$B_0 = \frac{m_e c^2}{8k}.$$

In function (1), A represents the whole instrumental coefficient which is identical in both Thomson and Raman measurements. This coefficient includes the efficiencies of solid angle, scattering length, and other optical efficiencies such as the transmissivity of the view window. E is the pulse energy of the incident laser, n_e is the electron density. $d\sigma^T/d\Omega$ is the differential cross section of TS. f_1, θ, and β are the spectral responsibility of the channel 1, the angle between the direction of incident light and the scattered light, and the angle between the polarization of incident laser and observation direction, respectively. In our system, $\theta=90°$ and $\beta=90°$. Similarly, the Raman scattering signal S^R is given as[8]

$$S^R = AEn^N \sum_J w_j^N \frac{d\sigma_J^N}{d\Omega} f_1(\lambda_J^N). \tag{3}$$

N stands for nitrogen and J is the initial rotational-angular-momentum quantum number. The wavelengths of Raman scattering peaks λ_J^N are given by[11]

$$\lambda_J = \lambda_0 - (4B - 6D)(J - 0.5) + 8D(J - 0.5), \tag{4}$$

w_j^N is the population of the initial rotational state.[12] For a gas in thermal equilibrium at a temperature T,

$$w_J^N = W^{-1} g_J (2J + 1)\exp[-J(J + 1)hcB/kT], \tag{5}$$

$$\sum_{J=0}^{\infty} w_J^N = 1. \tag{6}$$

For the nitrogen, $B=1.99\times10^2$ m^{-1} and $D=5.74\times10^{-4}$ m^{-1}, $d\sigma_J^N/d\Omega$ is the differential cross section of the anti-Stokes rotational $J'=J-2$ Raman transition, and which can be written as[12,13]

$$\frac{d\sigma_J^N}{d\Omega} = \sigma_{zz}[(1 - \rho)\cos^2\psi + \rho], \tag{7}$$

where ρ is the depolarization factor. The Raman-scattered light is largely unpolarized and the theoretical value of the depolarization ρ is 3/4. ψ is the angle between the polarizations of incident and scattered lights, and in our system it is 90°.[12]

$$\sigma_{zz} = \frac{64\pi^4}{45} \frac{3J(J-1)}{2(2J+1)(2J-1)} \frac{\gamma^2}{\lambda_J^4}. \tag{8}$$

The value of the anisotropy of the molecular polarizability γ is estimated about 0.66×10^{-30} m^3 at the incident wavelength of 1064 nm by linear extrapolation from experimental data.[3,11] J is the rotation state. For the nitrogen Raman scattering, $J=6$ and 3 when J is even and odd, respectively.

Since the effective cross section of Raman scattering falls exponentially, the Raman signals can be detected by only channel 1 in the polychromator. Figure 3 shows the spectral responsibilities of channel 1 together with effective cross section distributions of the rotational Raman lines for molecular nitrogen.

Rearanging Eq. (1) by substituting the solution of Eq. (3) for A, E,

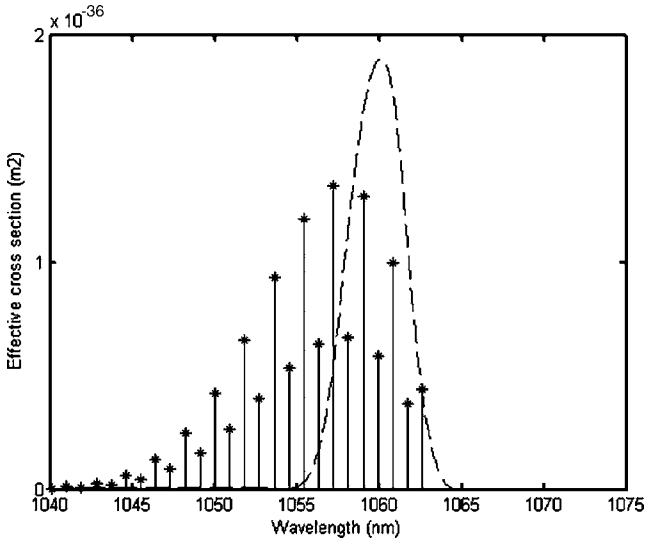

FIG. 3. Spectral responsibility of the channel 1 and effective Raman cross sections for molecular nitrogen.

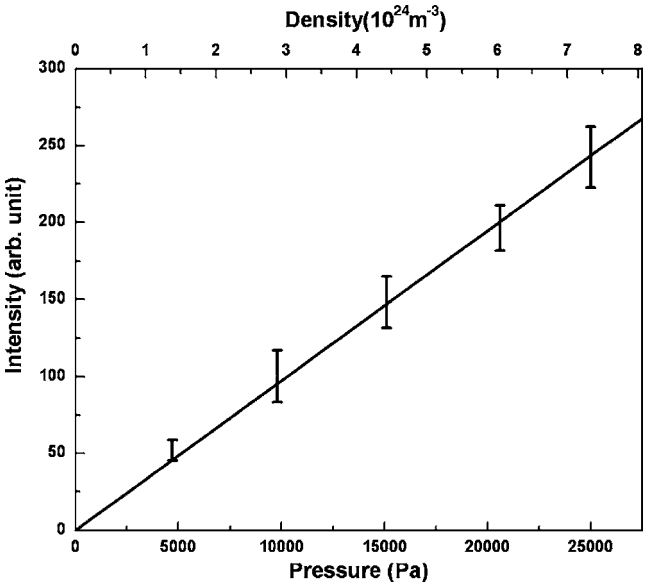

FIG. 4. Density dependence of the Raman signals measured by the polychromator. The calibration factor is defined by the gradient of the fit line.

$$n_e = \frac{n^{\mathrm{N}}}{S^R}\frac{S^T P^R}{P^T}, \tag{9}$$

$$P^R = \sum_J w_j^{\mathrm{N}} \frac{d\sigma_J^{\mathrm{N}}}{d\Omega} f_1(\lambda_J^{\mathrm{N}}), \tag{10}$$

$$P^T = \frac{d\sigma^T}{d\Omega}\int S(\lambda, T_e) f_1(\lambda) d\lambda, \tag{11}$$

n^{N}/S^R can be calibrated by Raman scattering experiment. In the Raman calibration, we fill the HT-7 vacuum vessel with nitrogen gas and measure Raman signal intensities at six pressure values from 5000 to 20 000 Pa, respectively, to determine the quantity n^{N}/S^R. The air pressure is monitored with a capacitance manometer installed on the HT-7. Figure 4 shows the density dependence of the Raman signal detected by channel 1 in the polychromator. The Raman signals from 60 laser pulses are accumulated to decrease the statistical uncertainty. As expected, the signal intensity is proportional to the air density. The calibration coefficients for the polychromator can be obtained from the gradient of the fit line.

The errors are mainly attributed to following aspects. The first error is originated from the estimation of P^R which denotes the degree of overlapping of the spectral responsibility and Raman cross section distribution. The cross section error is about ±8%, it is induced from the polarizability anisotropy having an uncertainty of ±4% for molecular nitrogen. In addition, the absolute position of the spectral responsibility f_1 measured includes some uncertainties. Only a small part of the Raman spectrum can be observed from the polychromator whose cross sections are small, as shown in Fig. 3. Therefore, the value of P^R is very sensitive to the relative position of the spectral responsibility to Raman lines, which causes an inaccuracy. We have estimated the uncertainty of $f_1(\lambda_J^{\mathrm{N}})$ to be about ±5%. The second error comes from P^T as it is the function of the electron temperature T_e which itself has a calculated error of ±10%. Thirdly, the calibration factor n^{N}/S^R has an error of less than 5%. Lastly, statistical uncertainty in S^T depends on the detected photon number of Thomson scattered light, and is typically ±5% or less. From the considerations above, total uncertainty has been estimated to be ±18%.

IV. ELECTRON DENSITY MEASUREMENTS

The electron temperature and density of HT-7 central plasmas can be measured with the calibrated YAG Thomson scattering system. Figure 5 shows a lower hybrid wave (LHW) and ion Bernstein wave (IBW) combined plasma discharge in HT-7 superconducting Tokamak. The total power of LHW and IBW up to 1 MW has been successful injected.

It has been found that the values of electron temperature increased with the LHW and IBW injected. Figure 6 gives the results of temperature and density of the central plasma dependence on time. For the time being, there is only one Thomson scattering channel in HT-7 Tokamak. Moreover, there is no sufficient millimeter-wave (MMW) interferometer information to support Abel invert. As a result, it is difficult to find any other method to support the density results calculated from our diagnostic system. However, the experiments have been repeated for several times, similar electron density values and time-dependence trends are obtained. In addition, the accuracy is limited to 18%. All these demonstrate the reliability of our results.

V. SUMMARY AND DISCUSSION

We have successfully calibrated the HT-7 YAG Thomson scattering system by using anti-Stokes rotational Raman scattering from nitrogen gas in this work. The fundamental scattering properties have been well established. Serials of electron densities obtained show good repeatability. The exact temperature and density measured by this system will

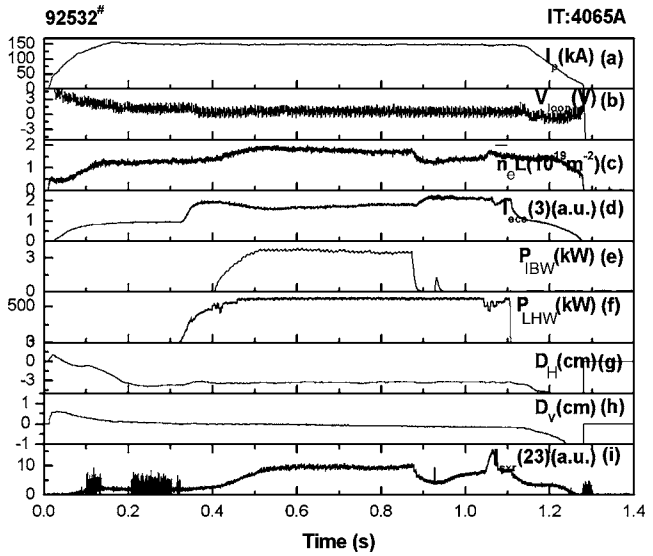

FIG. 5. A typical LHW and IBW combined plasma discharge. (a) Plasma current; (b) loop voltage; (c) MMW interferometer measures line integrated (a vertical chord at $R=1.22$ m) electron density at a horizontal port as the YAG Thomson scattering; (d) ECE intensity from channel 8; (e) the LBW power (f) the LHW power; (g) R position, horizontal displacement of the center of the last closed magnetic flux surface from two different equilibrium calculation programs; (h) Z position, vertical displacement of the center of the last closed magnetic flux surface from two different equilibrium calculation programmers; (i) soft x-ray intensity from channel 23 (central channel).

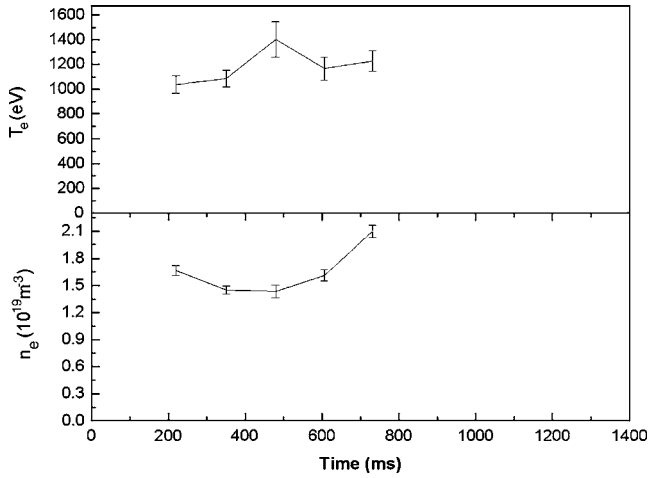

FIG. 6. Electron temperature and electron density.

serve important information on the physics properties of Tokmak plasmas. In our next work, this calibration technical will be employed on EAST Thomson scattering technology.

ACKNOWLEDGMENTS

This work was partly supported by the JSPS-CAS Core-University Program on Plasma and Nuclear Fusion. Also, it was funded by the National Nature Science Foundation of China with Contract Nos. 10675126 and 10375068.

[1] J. S. Mao, J. Y. Zhao, and Y. D. Li, Plasma Sci. Technol. **3**, 691 (2001).
[2] Q. Zang, J. Y. Zhao, and G. Q. Yun, "Multipulse Thomson scattering diagnostic on the HT-7 Tokmak," Plasma Sci. Technol. (to be published).
[3] M. J. v. d. Sande, "Laser scattering on low temperature plasmas—high resolution and stray light rejection," thesis, Technische Universiteit Eindhoven, 2002.
[4] T. Yamauchi and I. Yanagisawa, Appl. Opt. **24**, 700 (1985).
[5] H. Rönr, Phys. Lett. A **60**, 185 (1977).
[6] H. Rönr, Phys. Lett. A **81**, 451 (1981).
[7] J. Howard, B. W. James, and W. I. B. Smith, J. Phys. D **12**, 1435 (1979).
[8] I. Yamada, K. Narihara, and H. Hayashi, Rev. Sci. Instrum. **74**, 1675 (2003).
[9] B. F. M. Potz, J. J. H. Coumans, and D. C. Schram, Phys. Fluids **24**, 517 (1981).
[10] J. Sheffield, Plasma Phys. **8**, 783 (1972).
[11] K. Narihara, Fusion Eng. Des. **34**, 67 (1997).
[12] C. M. Penny, R. L. S. Peters, and M. Lapp, J. Opt. Soc. Am. **64**, 712 (1974).
[13] R. W. Carlson and W. R. Fenner, Astrophys. J. **178**, 551 (1972).